Journal Pre-proofs

In vivo preclinical evaluation of the new ^{68}Ga-labeled beta-cyclodextrin in prostaglandin E2 (PGE2) positive tumor model using positron emission tomography

György Trencsényi, Adrienn Kis, Judit P. Szabó, Ágnes Ráti, Katalin Csige, Éva Fenyvesi, Lajos Szente, Milo Malanga, Gábor Méhes, Miklós Emri, István Kertész, Miklós Vecsernyés, Ferenc Fenyvesi, István Hajdu

PII: S0378-5173(19)30999-8
DOI: https://doi.org/10.1016/j.ijpharm.2019.118954
Reference: IJP 118954

To appear in: *International Journal of Pharmaceutics*

Received Date: 10 October 2019
Accepted Date: 11 December 2019

Please cite this article as: G. Trencsényi, A. Kis, J.P. Szabó, A. Ráti, K. Csige, E. Fenyvesi, L. Szente, M. Malanga, G. Méhes, M. Emri, I. Kertész, M. Vecsernyés, F. Fenyvesi, I. Hajdu, *In vivo* preclinical evaluation of the new ^{68}Ga-labeled beta-cyclodextrin in prostaglandin E2 (PGE2) positive tumor model using positron emission tomography, *International Journal of Pharmaceutics* (2019), doi: https://doi.org/10.1016/j.ijpharm.2019.118954

In vivo preclinical evaluation of the new ^{68}Ga-labeled beta-cyclodextrin in prostaglandin E2 (PGE2) positive tumor model using positron emission tomography

György Trencsényi[a*], Adrienn Kis[a], Judit P. Szabó[a], Ágnes Ráti[a], Katalin Csige[a], Éva Fenyvesi[b], Lajos Szente[b], Milo Malanga[b], Gábor Méhes[c], Miklós Emri[a], István Kertész[a], Miklós Vecsernyés[d], Ferenc Fenyvesi[d1], István Hajdu[a1]

[a]Division of Nuclear Medicine and Translational Imaging, Department of Medical Imaging, Faculty of Medicine, University of Debrecen, Nagyerdei St. 98, H-4032 Debrecen, Hungary

[b]Cyclolab Cyclodextrin R&D Laboratory Ltd., H-1097, Illatos St. 7, Budapest, Hungary

[c]Department of Pathology, Faculty of Medicine, University of Debrecen, Nagyerdei St. 98, H-4032 Debrecen, Hungary

[d]Department of Pharmaceutical Technology, Faculty of Pharmacy, University of Debrecen, Nagyerdei St. 98, H-4032 Debrecen, Hungary

[1] These authors contributed equally to this study.

* corresponding author

Corresponding author:

György Trencsényi, PhD; Division of Nuclear Medicine, Department of Medical Imaging, Faculty of Medicine, University of Debrecen, Nagyerdei St. 98, H-4032 Debrecen, Hungary

E-mail: trencsenyi.gyorgy@med.unideb.hu

Abstract

The cyclooxygenase-2 (COX-2)/prostaglandin E2 (PGE2) pathway plays an important role in tumor development and formation of metastases. It was earlier reported that cyclodextrin derivatives have a high affinity to form complexes with PGE2. Based on these results radiolabeled cyclodextrins – as new radiopharmaceuticals – may open a new pathway in the *in vivo* imaging and diagnosis of PGE2 positive tumors. The aims of this study were to synthetize the PGE2 specific ^{68}Ga-labeled NODAGA-randomly methylated beta-cyclodextrin (^{68}Ga-NODAGA-RAMEB) and investigate its tumor-targeting properties. NODAGA-RAMEB was labeled with Gallium-68 (^{68}Ga), and the radiochemical purity (RCP%), partition coefficient (log*P* values), and *in vitro-in vivo* stability of ^{68}Ga-NODAGA-RAMEB were determined. After intravenous injection of ^{68}Ga-NODAGA-RAMEB the accumulation in organs and tissues was monitored *in vivo* by positron emission tomography (PET) and *ex vivo* by gamma counter in BxPC-3 and PancTu-1 tumor-bearing CB17 SCID mice. The RCP% of the newly synthesized ^{68}Ga-NODAGA-RAMEB was higher than 98%. The molar activity was 15.34±1.93 GBq/μmol. The log*P* of ^{68}Ga labeled NODAGA-RAMEB was −3.63±0.04. Biodistribution studies showed high accumulation of ^{68}Ga-NODAGA-RAMEB in PGE2 positive BxPC-3 tumors; approximately 15-20-fold higher radiotracer uptake was observed, than that of the background. ^{68}Ga-labeled RAMEB is a promising radiotracer in PET diagnostics of PGE2 positive tumors.

Keywords: ^{68}Ga; cyclodextrin; Positron Emission Tomography; prostaglandin E2

Abbreviations

COX-2	cyclooxygenase-2
DIPEA	*N,N*-Diisopropylethylamine
DMSO	dimethyl sulfoxide
EP	E-type prostanoid receptor
HPβCD	(2-Hydroxypropyl)-β-cyclodextrin
i.v.	intravenous(ly)
log*P*	octanol – water partition coefficient
MS	mass spectrometer
Mw	molecular weight
NODAGA	p-NCS-benzyl-NODA-GA
PET	positron emission tomography
PGE2	prostaglandin E2
RAMEB	randomly methylated β-cyclodextrin
RCP	radiochemical purity
RCY	radiochemical yield
RP-HPLC	reversed-phase high-performance liquid chromatography
u.p.	ultra-pure

1. Introduction

Nowadays, the research and application of cyclodextrin derivatives in the medical and pharmaceutical industries is increasing. These glucose-based cyclic oligosaccharides, due to their lipophilic central cavities and hydrophilic outer surfaces help to deliver molecules with low water solubility through the cell membrane (Loftsson et al., 2005). Because of these properties, cyclodextrins are widely used as pharmaceutical excipients in the formulation of hydrophobic drugs (Arima et al., 2017; Frömming and Szejtli, 1994; Szejtli, 1998) and as nanoparticle-based drug delivery systems for many years (Calias, 2017; Duchene et al., 2016). It is known that cyclodextrin derivatives are effective in the therapy of several diseases. Among different types of cyclodextrins, 2-hydroxypropyl-β-cyclodextrin (HPβCD) is used as a therapeutic intervention for Niemann-Pick type C1 disease (Ottinger et al., 2014) and this compound increases cholesterol solubility in atherosclerosis (Zimmer et al., 2016), furthermore, preclinical data suggest that HPβCD is a promising anticancer agent for acute and chronic myeloid leukemia (Yokoo et al., 2015).

It was earlier reported that prostaglandin E2 (PGE2) binds randomly methylated β-cyclodextrin (RAMEB) with high affinity and this observation may be of great importance in the therapy of PGE2 induced inflammatory hyperalgesia (Sauer et al., 2017). The cyclooxygenase-2 (COX-2)/PGE2 axis and the PGE2 receptors play crucial role not only in inflammation, but also in carcinogenesis. The overexpression of cyclooxygenase-2 (COX-2) and its enzymatic product prostaglandin E2 (PGE2) are involved in cancer progression and development of therapeutic resistance. The deregulation of COX-2/PGE2 pathway participates in tumor initiation, promotes tumor maintenance and the formation of metastatic lesions. Furthermore, several studies have shown that the overexpression of COX-2 and PGE2 in tumor microenvironment is associated with poor prognosis and largely reducing the length of patient survival (Greenhough et al., 2009; Zmigrodzka et al., 2018). PGE2 acts through four different G-protein coupled plasma membrane receptors (E-type prostanoid receptors: EP1-4) and has been linked to the development and survival of tumors. Among EP receptors EP1 and EP2 receptors require significantly higher levels of PGE2 for the activation. It has been shown that the PGE2-induced EP1 and EP2 receptor signaling is involved in tumor proliferation by suppressing the cells of anti-tumor immunity (dendritic cells (DCs), natural killer (NK) and T cells), inhibiting apoptosis and promoting tumor associated neo-angiogenesis and help tumors to adapt to hypoxia (O'Callaghan and Houston, 2015; Liu et al., 2015). All of these effects lead to the

survival of tumor cells and the development of distant metastases. Due to the high expression of PGE2 and its receptors in different human malignancies as renal tumors (Verratti et al., 2019), hematological tumors (Zmigrodzka et al., 2018), osteosarcoma (Zhou et al., 2019), colorectal tumors (Park et al., 2018), hepatocellular carcinoma (Koga et al., 1999), breast cancer (Li et al., 2015), pancreatic cancer (Tong et al., 2018) and glioblastoma (Jiang et al., 2017), PGE2 is a novel and intensively investigated molecular target in anticancer therapy (O'Callaghan and Houston, 2015; Reader et al., 2011; Tong et al., 2018) and can be a prognostic biomarker of different cancers and, in addition, a new target for *in vivo* molecular imaging of tumors in the field of nuclear medicine.

Positron emission tomography (PET) is one of the most frequently used imaging techniques among non-invasive *in vivo* diagnostic modalities for the detection of primary tumors and metastases in human patients and also in preclinical studies using experimental animals. Due to specific radiopharmaceuticals, PET has a high sensitivity for detecting tumorous lesions. With the advancement of molecular biology and the discovery of new tumor-related targets, the development of tumor-specific radiopharmaceuticals for PET diagnostics is also progressing rapidly. In the synthesis of radiopharmaceuticals, radiochemistry applies different radiometals and non-metallic based radionuclides. Among radiometals, the short-lived, positron emitter ^{68}Ga (t1/2 = 68 min) is widely used for the synthesis of diagnostic probes, because it is easily accessible using commercially available ^{68}Ge/^{68}Ga generator. ^{68}Ga is a useful radiometal for labeling tumor and receptor specific peptides such as prostate specific membrane antigen (PSMA) in prostate cancer (Giovacchini et al., 2018), α-*MSH* analog in melanoma (Nagy et al., 2017), and suitable for labeling other molecules e.g. nanoparticles (Körhegyi et al. 2019) and cyclodextrins (Hajdu et al., 2019). The aims of this study were to synthetize the PGE2 specific ^{68}Ga-labeled NODAGA-randomly methylated beta-cyclodextrin (68Ga-NODAGA-RAMEB) and investigate the tumor-targeting properties and the *in vivo* biodistribution of this new radiolabeled probe using the non-invasive PET imaging.

2. Materials and methods

2.1. Chemicals

6-Monodeoxy-6-monoamino-randomly-methylated-beta-cyclodextrin hydrochloride (NH_2-RAMEB) was produced by CycloLab Ltd. (Cat. No.: CY-2056; Budapest, Hungary). p-NCS-benzyl-NODA-GA (NODAGA) was obtained from CheMatech (Cat. No.:C103) (Dijon, France). For the chemical synthesis the dimethyl sulfoxide (DMSO), *N,N*-Diisopropylethylamine (DIPEA) and for the ^{68}Ga labeling procedures the ACS grade water and ammonium acetate (NH_4OAc) was acquired from Sigma-Aldrich Kft. (Budapest, Hungary). Ultra-pure (u.p.) HCl was the product of Merck Kft. (Budapest, Hungary). Prostaglandin E2 (PGE2; Cat.No.: 3632464) was purchased from Biogems Int. USA. All other chemicals were purchased from VWR International Kft. (Debrecen, Hungary) and Sigma-Aldrich Kft. (Budapest, Hungary) and they were used without further purification.

2.2. Conjugation of the NODAGA chelator with NH_2-RAMEB

NODAGA complexing agent was conjugated *via* the amino group to NH_2-RAMEB based on the protocol described earlier (Hajdu et al 2019). Briefly, NH_2-RAMEB (20 mg, 16.6 μM) was dissolved in water (4 mL) and the solution was cooled to 4 °C and stirred for 15 minutes. NODAGA (9.9 mg, 16.6 μM) was dissolved in DMSO (250 μL) and the solution was added to the cooled NH_2-RAMEB solution under stirring. The pH of the reaction mixture was adjusted to 8.5 by adding DIPEA dropwise. The reaction mixture was stirred for 24 hours at room temperature. The product was lyophilized, re-dissolved and purified on a KNAUER HPLC system with a Supelco Discovery® BIO Wide Pore semi preparative C-18 column (L × I.D.: 150 mm × 10 mm, particle size: 10 μm). The mobile phase was composed of solvent A (0.1% trifluoroacetic acid (TFA) in water) and solvent B (0.1% TFA in acetonitrile-water (95:5, v/v)). The flow rate was 4 mL/min, detection was performed using a KNAUER absorbance detector at 254 nm. The gradient of solvent A started with 85% to 85% at 2 min to 60% at 20 min to 35% at 25 min. Synthesis yield was 74%. The purity of the NODAGA-RAMEB was verified on a KNAUER HPLC using Supelco Discovery® Bio Wide Pore C-18 column (250 mm × 4.6 mm; particle size: 10 μm). Gradient elution was achieved at a flow rate of 1 mL/min. The mobile phase was composed of solvent A (0.1% TFA in water) and solvent B (0.1% TFA in

acetonitrile-water (95:5, v/v)). Signals were detected using a KNAUER absorbance detector at 254 nm. The gradient of solvent A started with 100% to 10% at 15 min to 10% at 17 min to 100% at 20 min. The exact molecular weight was confirmed with high-resolution mass spectrometry (MS) (maXis II UHR ESI-TOF MS, Bruker Corp. Billerica, Massachusetts, USA). The structure of the product was verified with nuclear magnetic resonance (NMR) (Bruker 400 MHz spectrometer, Bruker Corp. Billerica, Massachusetts, USA). Finally, 1 mM stock solution was prepared from the certified product (NODAGA-RAMEB) in ultra-pure water for the radiolabeling reactions.

2.3. Gallium-68 labeling of NODAGA-RAMEB

A ^{68}Ge/^{68}Ga generator (50 mCi, Gallia-Pharm, Eckert and Ziegler Germany) was eluted with 5 mL 0.1 M u.p. HCl. The highest activity aliquot (1 mL) was buffered with sodium acetate (1 M, 160 µl) to ensure a pH of 4.3−4.5, followed by the addition of an aqueous solution of NODAGA-RAMEB (1 mM, 10 µL). The reaction mixture was heated at 95 °C for 10 min. Thereafter, the solution was transferred to a Light C18 Sep-Pak Cartridge and was washed with water (2 mL) to remove the buffer. The ^{68}Ga-labeled NODAGA-RAMEB (^{68}Ga-NODAGA-RAMEB) product was eluted with 0.5 ml of 96% EtOH/isotonic NaCl solution 1:2 mixture. For evaluating the radiochemical purity the aforementioned HPLC system with Supelco Discovery® Bio Wide Pore C-18 column (250 mm × 4.6 mm; particle size: 10 µm) was used, but combined with a radio detector. Signals were simultaneously detected by both radio and absorbance detector at 254 nm. The product was diluted with saline solution to decrease the ethanol-content below 10% and was sterile filtered before using for animal experiments.

2.4. Determination of partition coefficient (log*P*)

The ^{68}Ga-NODAGA-RAMEB (10 µL, 5.5±0.2 MBq) was mixed with a mixture of 1-octanol (500 µL) and PBS solution (490 µL, pH 7.4) in an Eppendorf tube. To assess the Log*P* of the inclusion complex also, in a separate experiment ^{68}Ga-NODAGA-RAMEB (20 µL, 9.3±0.3 MBq) and PGE2 (1 mg in 10 µL ethanol) was added to 1-octanol (490 µL) and PBS solution (480 µL) and mixed. The mixtures were stirred vigorously for 20 min at room temperature and then centrifuged at 20.000 rpm/min for 5 min at 4 °C for complete separation of the layers. Precise amounts of samples (100 µL in triplets) were pipetted out from the separated layers and were taken into test tubes. The radioactivity was measured with a calibrated gamma counter (Perkin-Elmer Packard Cobra, Waltham, MA, USA). Experiments were carried out twice with triplicate samples.

2.5. Determination of *in vitro* and *in vivo* metabolic stability

The *in vitro* stability of ^{68}Ga-NODAGA-RAMEB was tested in mouse serum. ^{68}Ga-NODAGA-RAMEB (10.0±0.5 MBq) was added into mouse serum and were incubated at 37 °C without stirring. Samples from this mixture (50 µL) was mixed with ice-cold abs. ethanol (50 µL) at different time points (30, 60, 90 and 120 min) and centrifuged at 10.000 rpm for 5 min at 4 °C. The supernatant was collected, diluted with water and evaluated with analytical radio-HPLC. The *in vivo* metabolic stability was measured in healthy SCID mice. ^{68}Ga-NODAGA-RAMEB was administered (7.5±0.4 MBq) into mice *via* the tail vein. The urine samples were collected at 60 min post injection. The obtained sample (50 µL) was mixed with ice-cold abs. ethanol (50 µL) and centrifuged at 10 000 rpm for 5 min. The supernatant was analyzed by analytical radio-HPLC. In both cases the HPLC chromatograms were compared to the initial chromatograms of the intact radiotracer to find any new radio-metabolite forms.

2.6. Investigation of the ^{68}Ga-NODAGA-RAMEB and PGE2-conjugated resin binding reaction

H-Gly-HMPB-ChemMatrix® resin (750 mg, 0.3-0.65 mmol/g) was dwelled in DCM (5 mL) for 10 minutes. Prostaglandin E2 (38.8 mg, 0.11 mmol, PGE2), PyBOP (62.5 mg, 0.12 mmol) and DIPEA (21 µL, 0.12 mmol) were added and the mixture was stirred for 2 hours. After completion of the reaction, the resin was filtered by means of a glass-filter, was rinsed twice with cold DCM (5 mL) and evaporation until dryness yielded the conjugated resin (775 mg). The overall yield of the coupling reaction was 98%. Thereafter, in parallel experiments, unmodified resin (10 mg) and PGE2 conjugated resin (10 mg) were placed into a polypropylene (PP) barrel (1 mL), equipped with a PP frit. 700-700 µl of PBS was introduced and after 3 minutes, ^{68}Ga-NODAGA-RAMEB (35±5 MBq) (40 µL) was injected to each sample and they were incubated for 10 min at room temperature during gentle shaking. After the incubation, the resins were filtered and were rinsed with additional PBS (1 mL). The activities of the resins and the supernatants were measured.

2.7. Experimental animals

CB17 SCID immunodeficient mice (12-week-old male mice were purchased from Innovo Ltd,

Hungary; n=35) were used for the *ex vivo* and *in vivo* experiments. Mice were housed under sterile conditions in IVC cage system (Techniplast, Italy) at a temperature of 26±3°C, with 52±10% humidity and artificial lighting with a circadian cycle of 12h. Sterile semi-synthetic diet (Akronom Ltd., Budapest, Hungary) and sterile drinking water were available *ad libitum* to all the animals. Laboratory animals were kept and treated in compliance with all applicable sections of the Hungarian Laws and regulations of the European Union.

For the induction of tumor models BxPC3 (ATCC, CRL-168) or PancTu-1 (kind gift from the University of Hamburg) human pancreas adenocarcinoma cells were injected ($5x10^6$ cells in 100 µL 0.9% NaCl) subcutaneously into the left shoulder area of CB17 SCID mice. *Ex vivo* and *in vivo* biodistribution studies were carried out 12±1 days after subcutaneous injection of tumor cells at the tumor volume of 95±8 mm^3.

2.8. Small animal PET imaging

Healthy control and approximately 12 days after tumor cell inoculation BxPC3 and PancTu-1 tumor-bearing animals were anaesthetized by 3% isoflurane (Forane) with a dedicated small animal anesthesia device (Eickemeyer Research, Tec3, Ghislandi Kft., Hungary) and were injected with 7.3±0.3 MBq ^{68}Ga-NODAGA-RAMEB *via* the lateral tail vein. In other experiments PGE2 positive BxPC3 tumor-bearing SCID mice were injected intravenously with 7.25±0.21 MBq of ^{68}Ga-NODAGA-RAMEB mixed with 1 mg PGE2 in 100 µL saline containing 4% ethanol. After the injections *in vivo* static and dynamic (0-90min) PET imaging were performed for the determination of the *in vivo* biodistribution of the radiotracer using the MiniPET-II small animal PET scanner under inhalation anesthesia.

2.9. PET data analysis

Ellipsoidal 3-dimensional volumes of interest (VOI) were manually drawn around the edge of the organ activity by visual inspection using BrainCad image analysis software. For the quantitation of the radioactivity concentration in the investigated tumors, organs and tissues standardized uptake value (SUV) was calculated as follows: SUV = [VOI activity (Bq/mL)]/[injected activity (Bq)/animal weight (g)], assuming a density of 1 g/mL. Tumor-to-muscle (T/M) ratios were calculated from the SUVmean of tumor and SUVmean of the background (muscle).

2.10. *Ex vivo* organ distribution studies

For *ex vivo* biodistribution studies control and tumor-bearing (BxPC3 or PancTu-1) SCID mice were injected intravenously with 7.31±0.32 MBq ^{68}Ga-NODAGA-RAMEB and 30, 60 and 90 min post injection animals were euthanized with 5% isoflurane. In other examinations BxPC3 tumor-bearing mice were injected with the mixture of ^{68}Ga-NODAGA-RAMEB (approx. 7 MBq) and 1 mg PGE2 in 100 µL saline containing 4% ethanol via the tail vein and 90 min post injection animals were euthanized with 5% isoflurane. Three tissue samples were taken from selected organs and their weight and the radioactivities were measured with a calibrated gamma counter (Perkin-Elmer Packard Cobra, Waltham, MA, USA). The ^{68}Ga-NODAGA-RAMEB uptake was expressed as %ID/g tissue.

2.11. Immunohistochemistry

Four µm thick sections of the formaldehyde fixed and paraffin embedded BxPC3 and PancTu-1 xenograft tumors were exposed to the rabbit monoclonal Anti-Prostaglandin E Receptor EP2/PTGER2 antibody (Abcam, USA; cat.no.: ab167171) at a dilution of 1:1000 following deparaffination, rehydration and antigen retrieval (pH 6.0) as usual. A HRP-labeled anti-rabbit polymer antibody (Mach2, BioCare Medical, USA, cat.no. RHRP520) and the Envision DAB detection kit (DAKO-Agilent Technologies, USA) were used for detection and visualization of the specific antibody binding, followed by hematoxylin counterstaining. Microscopic images were taken by a Leica DM2500 research microscope equipped a DFC495 digital camera and the LAS imaging tool kit.

2.12. Statistical analysis

Significance was calculated by two-way ANOVA, Student's t-test (two-tailed) and Mann-Whitney U-test and the significance level was set at $p \leq 0.05$ unless otherwise indicated. Data are presented as mean±SD of at least three independent experiments.

3. Results

3.1. Chemistry

The synthetic scheme for the precursor is shown in Fig. 1A. NODAGA-RAMEB was prepared from NH_2-RAMEB by conjugation of a bifunctional chelator (p-NCS-benzyl-NODA-GA) suitable for gallium-68 labeling. The final product was obtained after HPLC purification with more than 98% purity and the structure was confirmed by ^{1}H NMR and UHR ESI-TOF Mass Spectrometer. ^{1}H NMR measurement was carried out in (DMSO)-d_6. Chemical shifts, δ, are reported in parts per million (ppm), referenced to the residual ^{1}H: DMSO-d_6 at 2.50 ppm. (Fig. 1B) The theoretical and measured mass of the synthesized products were in concordance, where NODAGA-RAMEB m/z: calculated mass: 1781.7283, found mass: 1781.7289 $[M]^{1+}$ (Fig. 1C).

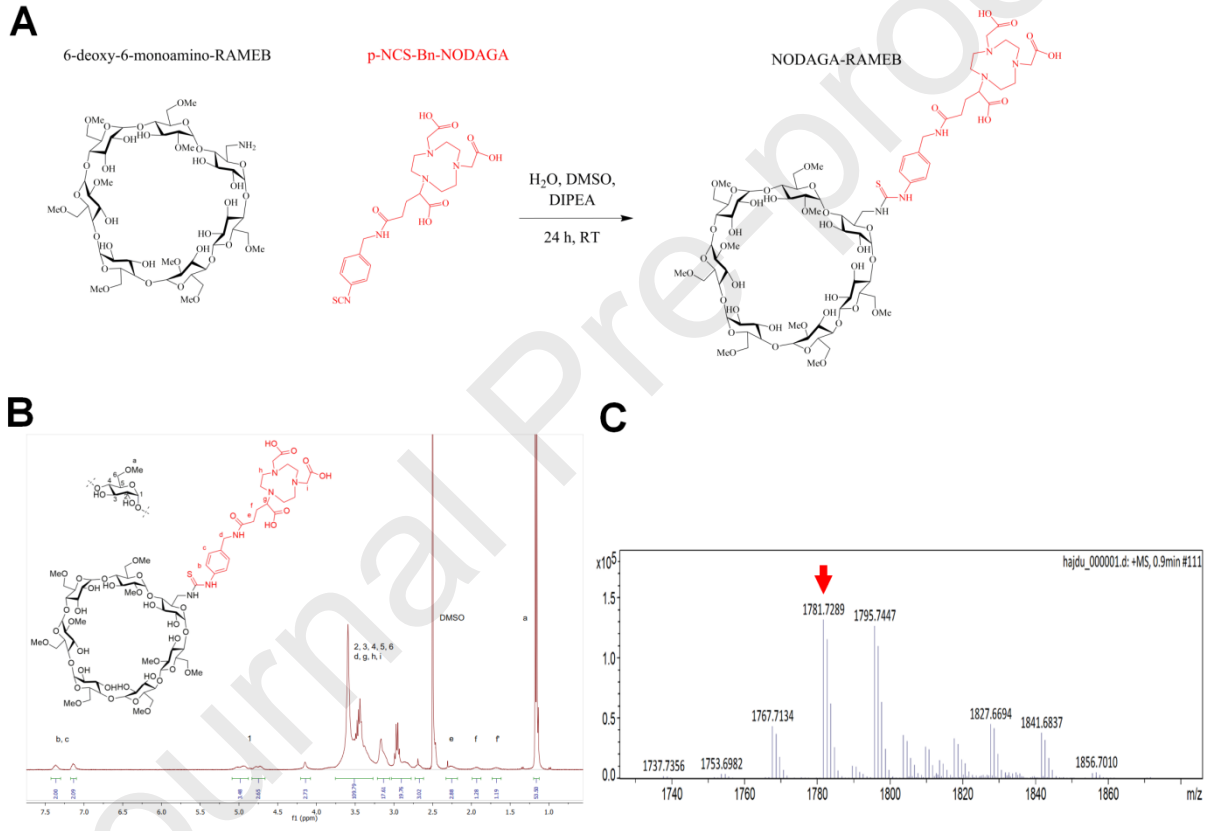

Fig. 1. Reaction scheme for the synthesis of NODAGA-RAMEB (A). ^{1}H NMR spectrum (B) and mass spectrum (C) of NODAGA-RAMEB.

3.2. Radiochemistry

The bifunctional chelator-conjugated cyclodextrin (NODAGA-RAMEB) was radiolabeled manually with $^{68}GaCl_3$ using 1 M sodium acetate buffer solution to obtain ^{68}Ga-labeled

NODAGA-RAMEB (Fig. 2). The overall reaction time was approximately 20 min. The molar activity was 15.34±1.93 GBq/μmol and the radiochemical purity (RCP) of the product was found over 98.0%. The retention time of the compound was 9.13 min (Fig. 2 B) on the applied analytical system.

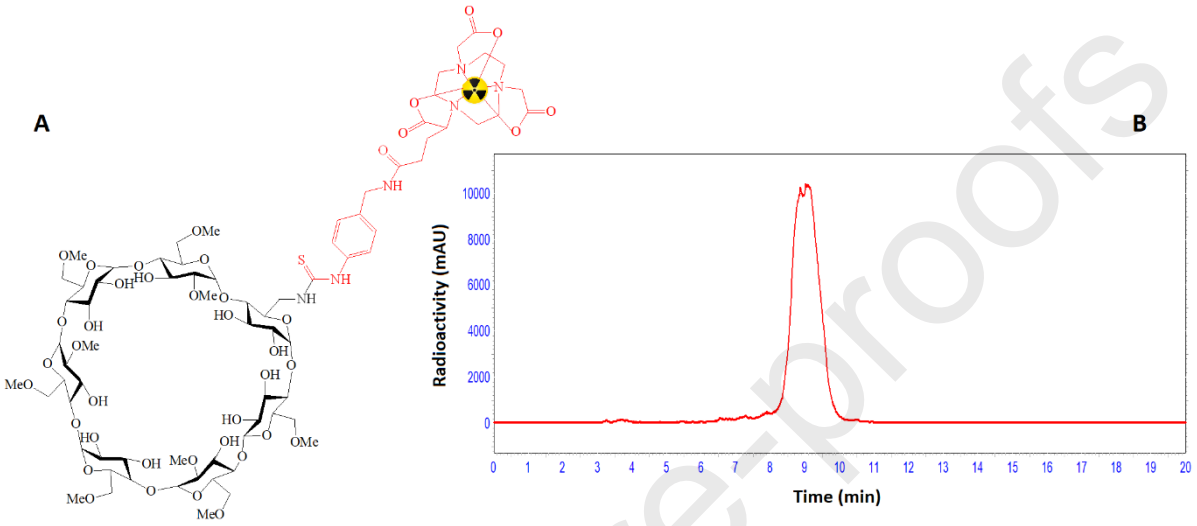

Fig. 2. Structure for the bifunctional chelator-conjugated cyclodextrin (A) and representative radio-HPLC chromatogram (B) of ^{68}Ga-NODAGA-RAMEB.

3.3. Determination of partition coefficient, resin binding and metabolic stability.

The log*P* value of ^{68}Ga-NODAGA-RAMEB was calculated to be -3.63±0.04, suggesting a very highly hydrophilic property. In experiments, where the log*P* value of ^{68}Ga-NODAGA-RAMEB inclusion complex was determined, it was found, that the hydrophilicity of the radiolabeled PGE2 complex moderately decreased - log*P* of -3.08±0.03. During the resin binding measurement the ^{68}Ga-NODAGA-RAMEB binding capacity of the resins was compared. It was found that the PGE2 conjugated resin bound 18.1±1.3% more ^{68}Ga labeled RAMEB than the unmodified resin suggesting the definite formation of the inclusion aggregate. The *in vitro* stability was determined in mouse serum at 37 °C using analytical radio-HPLC method. Samples were taken at 30, 60, 90 and 120 min and the ^{68}Ga-NODAGA-RAMEB remained stable during the measured period, and the radiochemical purity of the tracer proved to be over 99%. The *in vivo* stability was tested in urine collected from the mice after 1 hour radiotracer

administration. No measurable quantity of radioactive metabolite was found with radio-HPLC method, indicating excellent *in vivo* metabolic stability.

3.4. *In vivo* biodistribution studies in healthy control mice

For the determination of the ^{68}Ga-labeled NODAGA-RAMEB biodistribution in healthy control CB17 SCID mice dynamic PET imaging and *ex vivo* studies were performed. Representative dynamic PET images and the mean time-activity curve (TAC) are shown in Fig. 3 after intravenous injection of the radiolabeled probe. By the qualitative analysis of the decay-corrected PET images kidneys and bladder with urine (urinary system) were clearly visualized (Fig. 3A) and very low uptake was observed in other organs and tissues. 90 min post injection radioactivity only in the kidneys and in the bladder was identifiable and no background accumulation was observed. By the quantitative analysis of the PET images, the SUVmean data and the TAC (Fig. 3B) showed the rapid clearance of ^{68}Ga-NODAGA-RAMEB from the investigated organs. The radiotracer uptake of the investigated tissues significantly decreased after 5 minutes, and 90 min post injection very low ^{68}Ga-NODAGA-RAMEB accumulation was observed in the thoracic organs (SUVmean lung: 0.31±0.07, SUVmean heart: 0.12±0.04), in the abdominal region (SUVmean intestines: 0.13±0.03, SUVmean liver: 0.16±0.06, SUVmean stomach: 0.12±0.04) and in the brain (SUVmean: 0.12±0.04). Only the radioactivity of the urine increased significantly (SUVmean: 7.91±2.92 and 55.24±9.65; 5 and 90 min post injection, respectively).

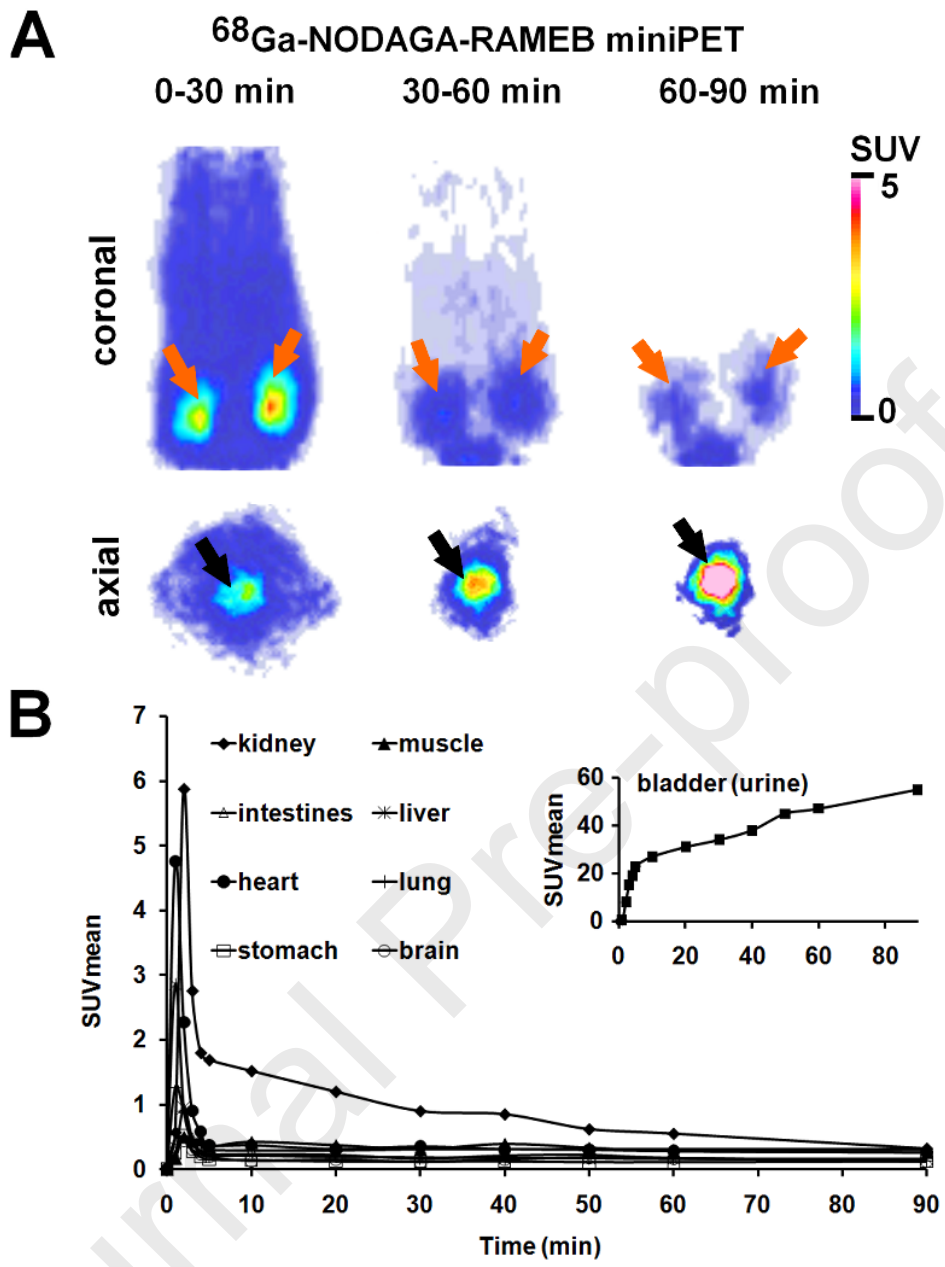

Fig. 3. *In vivo* biodistribution of the intravenously injected ^{68}Ga-NODAGA-RAMEB in healthy control SCID mouse. Representative decay-corrected dynamic PET images (A) and SUVmean time-activity curve (B) of ^{68}Ga-NODAGA-RAMEB in selected organs/tissues of a healthy SCID mouse. Orange arrows: kidneys; black arrows: urinary bladder.

3.5. *Ex vivo* biodistribution studies in healthy control mice

Ex vivo biodistribution studies were carried out after intravenous injection of ^{68}Ga-NODAGA-RAMEB and after 30, 60 and 90 min incubation times. The radiotracer uptake of the organs and tissues were assessed by a calibrated gamma counter. After the quantitative analysis of *ex vivo* results, we found that the *in vivo* SUV data correlated well with the *ex vivo* %ID/g values shown in Table 1. The %ID/g data revealed that the ^{68}Ga-NODAGA-RAMEB was rapidly cleared from the kidneys and increased in the bladder, confirming the highly hydrophilic properties of the ^{68}Ga-labeled cyclodextrin. No significant differences were found between the %ID/g values of the investigated time points (30, 60 and 90 min) when the ^{68}Ga-NODAGA-RAMEB accumulation of the urine, kidneys, intestines, fat, lung, and brain was determined. In other organs and tissues significant differences ($p \leq 0.01$) were found between the %ID/g values of 30 and 90 min when ^{68}Ga-NODAGA-RAMEB uptake was compared (Table 1). Overall, very low radiotracer accumulation was measured in the muscle, brain, fat, and pancreas. In addition, the *ex vivo* % ID/g data showed that the radiotracer accumulation – from 30 to 90 min – decreased in all of the investigated organs and tissues in a time dependent manner.

Table 1

Ex vivo biodistribution of ^{68}Ga-NODAGA-RAMEB (%ID/g) in healthy control SCID mice 30, 60 and 90 min after radiotracer injection. Significance level between 30 and 90 min: $p \leq 0.01$ (*). %ID/g values are presented as mean±SD.

Organ/tissue	30min (n=5)	60 min (n=5)	90min (n=5)
Blood	0.34±0.06	0.13±0.03	0.04±0.01*
Bladder (urine)	81.26±4.47	84.14±3.85	85.65±5.12
Liver	0.15±0.02	0.11±0.02	0.06±0.02
Spleen	0.14±0.03	0.09±0.02	0.04±0.01
Kidney	1.49±0.24	1.22±0.32	1.09±0.20
Small intestine	0.16±0.03	0.10±0.03	0.04±0.01*
Large intestine	0.16±0.05	0.14±0.03	0.07±0.02
Stomach	0.18±0.03	0.11±0.02	0.03±0.01*
Muscle	0.12±0.03	0.07±0.01	0.01±0.01*
Fat	0.06±0.01	0.05±0.01	0.05±0.02
Lung	0.28±0.08	0.21±0.04	0.14±0.03
Heart	0.14±0.03	0.07±0.01	0.03±0.01*
Brain	0.02±0.01	0.01±0.01	0.01±0.01
Bone	0.09±0.02	0.02±0.01	0.01±0.01*
Salivary glands	0.12±0.02	0.04±0.01	0.02±0.01*
Gall bladder	0.13±0.03	0.08±0.02	0.04±0.01*
Pancreas	0.08±0.02	0.05±0.01	0.01±0.01*

3.6. *In vivo* biodistribution studies in tumor-bearing SCID mice

The PGE2 selectivity of ^{68}Ga-NODAGA-RAMEB was investigated by *in vivo* dynamic PET imaging using subcutaneously growing BxPC3 and PancTu-1tumors 12±1 days after tumor cell inoculation. Representative decay-corrected small animal PET images are shown in Fig. 4. By the qualitative analysis of the PET images we found, that the subcutaneously growing BxPC3 tumors were clearly identifiable (Fig. 4A, red arrows) at 30 min post injection, however, with high background radioactivity. In addition, as the incubation time increased, the background activity decreased from 30 to 90 min, and the tumor became more prominent. This observation was confirmed by the quantitative SUV data analysis (Fig. 4B), where it was found that the T/M SUVmean data increased from 10 min (T/M SUVmean: 7.80±1.64) to 90 min (T/M SUVmean: 18.57±2.64) post injection. The SUVmean values of the BxPC3 tumors showed a very slow decrease from 10 minutes (SUVmean: 0.45±0.06 at 10 min) after the injection. Despite the relatively low radiotracer uptake of the BxPC3 tumors (SUVmean: 0.14±0.04 at 90

min), the high tumor-to-muscle ratio (T/M) resulted in an excellent image contrast. Different pharmacokinetic properties were observed when dynamic PET imaging was performed with the co-injection of ^{68}Ga-NODAGA-RAMEB and PGE2 in BxPC3 tumor-bearing mice. Figure 4 (C and D panel) shows that in the presence of PGE2, BxPC3 tumor is not identifiable at the first 5-10 min after the injection. Thereafter, the radiotracer accumulation in the BxPC3 tumor increases significantly with high SUV values (SUVmean: 0.95±0.20 at 30 min, and 1.12±0.21 at 90 min post injection). These SUVmean values are approximately 8-9-fold higher (significance: $p \leq 0.01$), than that of the ^{68}Ga-NODAGA-RAMEB accumulation at the same time without the co-injection of PGE2. In addition, significant accumulation of ^{68}Ga-NODAGA-RAMEB was observed in the background tissues (muscle, thoracic and abdominal organs) (Fig. 4C). This is indicated by a significantly ($p \leq 0.01$) and approximately 10-fold lower tumor-to-muscle ratio (T/M SUVmean: 1.36±0.15 and 1.56±0.23 at 30 and 90 min, respectively), than it was observed in the absence of the co-injected PGE2 molecule (Fig. 4B and D).

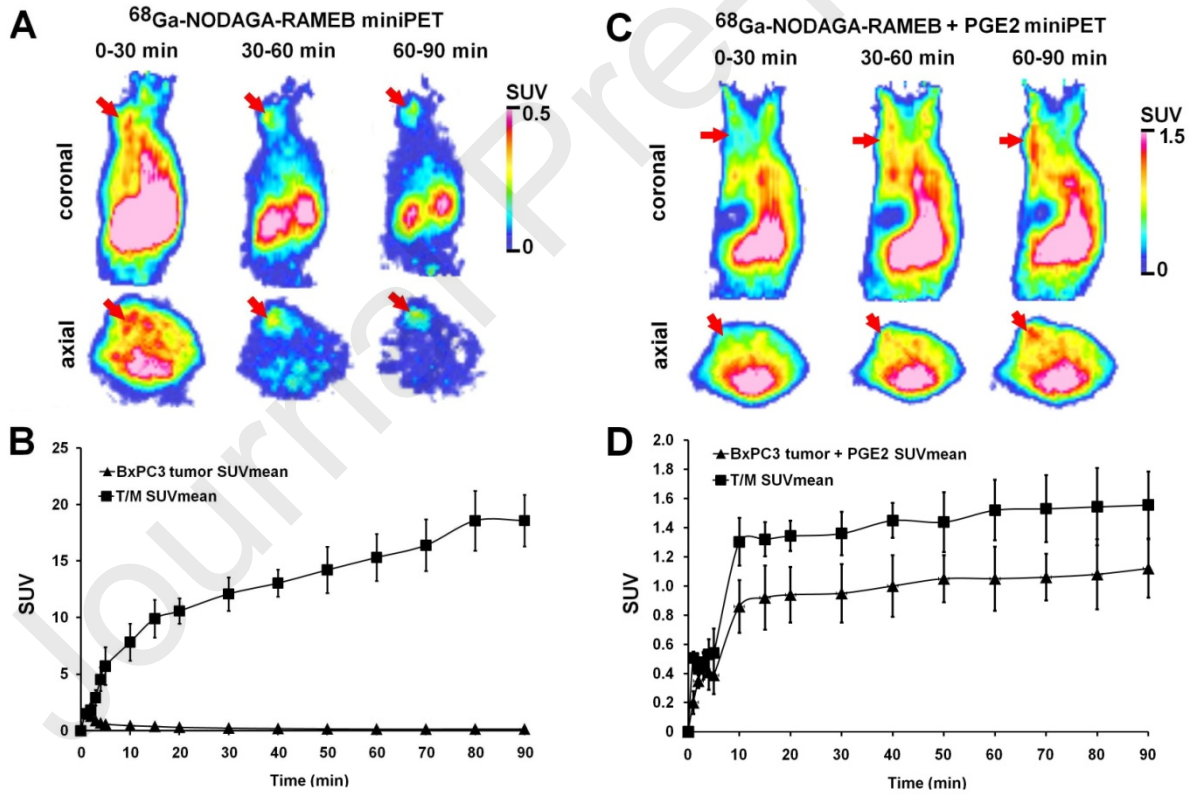

Fig. 4. *In vivo* dynamic miniPET imaging of BxPC3 tumor-bearing SCID mice after intravenous injection of ^{68}Ga-NODAGA-RAMEB (A, B) and ^{68}Ga-NODAGA-RAMEB+1 mg PGE2 (C, D). Representative time dependent decay-corrected coronal and axial miniPET images of BxPC3 tumor-bearing SCID mouse in the absence (A) and presence of PGE2 (C).

Time-activity curve (TAC) analysis of ^{68}Ga-NODAGA-RAMEB (B) and ^{68}Ga-NODAGA-RAMEB+1 mg PGE2 (D) accumulation in experimental PGE2 positive BxPC3 tumors. PET images and data were obtained 12±1 days after tumor cell inoculation. Red arrows: BxPC3 tumors. SUV: standardized uptake value; T/M: tumor-to-muscle ratio (SUVmean). SUV values are presented as mean±SD.

The PGE2 selectivity of ^{68}Ga-NODAGA-RAMEB was attested by using the low prostaglandin E2 receptor expressed PancTu-1 tumors. Representative decay-corrected PET images are shown in Fig. 5, 80-90 min post injection. By the qualitative analysis of the miniPET images it was found, that the BxPC3 tumors were clearly visualized (Fig. 5A, red arrows), however, the PancTu-1 tumor - with lower prostaglandin E2 receptor (EP2) expression - did not differ sharply from the background tissues (Fig. 5A, black arrows). 80-90 min after the *i.v.* injection of ^{68}Ga-NODAGA-RAMEB the SUVmean, SUVmax, T/M SUVmean and T/M SUVmax values of BxPC3 tumors were 0.15±0.04, 0.25±0.03, 18.85±2.64 and 18.32±3.21, respectively (Fig. 5B). By the assessment of the PET images at 80-90 min, we found significantly ($p \leq 0.01$) lower accumulation in the PancTu-1 tumors after using ^{68}Ga-NODAGA-RAMEB. The SUVmean (0.04±0.01), SUVmax (0.08±0.02), T/M SUVmean (1.33±0.19) and T/M SUVmax (1.66±0.22) values of PancTu-1 tumors were approximately 3-14-fold lower, than that of BxPC3 tumors, confirming the high PGE2 selectivity of the ^{68}Ga-labeled probe (Fig. 5B).

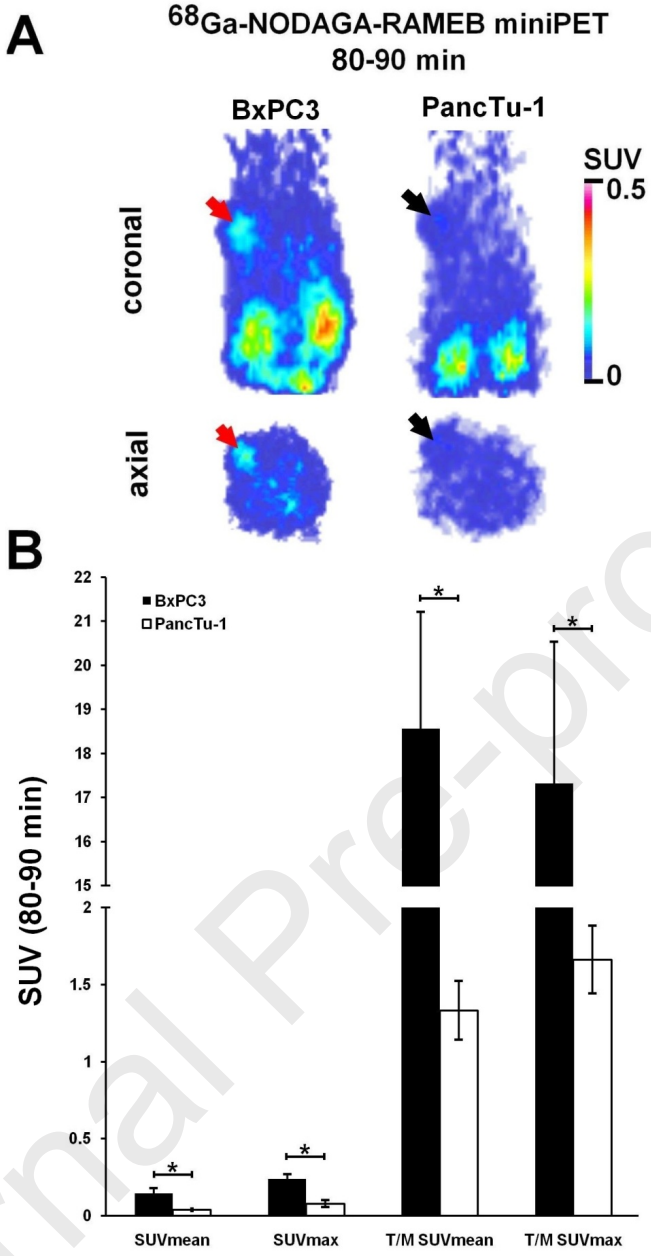

Fig. 5. *In vivo* assessment of ^{68}Ga-NODAGA-RAMEB accumulation of human pancreas adenocarcinoma cells using miniPET imaging. A: Representative decay-corrected coronal and axial miniPET images of BxPC3 (left) and PancTu-1 (right) tumor-bearing SCID mice 80-90 min after intravenous injection of ^{68}Ga-NODAGA-RAMEB. B: Quantitative SUV analysis of ^{68}Ga-NODAGA-RAMEB uptake in experimental tumors 80-90 min after intravenous injection of the radiotracer. PET images and data were obtained 12±1 days after tumor cell inoculation. Red arrows: BxPC3 tumors; black arrows: PancTu-1 tumors. SUV: standardized uptake value; T/M: tumor-to-muscle ratio (SUVmean and SUVmax). Significance level: $p \leq 0.01$ (*). SUV values are presented as mean±SD.

3.7. *Ex vivo* biodistribution studies in tumor-bearing SCID mice

For the assessment of PGE2 selectivity of ^{68}Ga-NODAGA-RAMEB *ex vivo* biodistribution studies were performed 30, 60 and 90 min post injection using BxPC3 tumor-bearing mice. Figure 6 demonstrates, that – except for the urinary system – the accumulation of ^{68}Ga-NODAGA-RAMEB in PGE2 positive BxPC3 tumors and the tumor-to-muscle ratios (T/M) were significantly ($p \leq 0.01$) higher at each investigated time point, than that of other organs and tissues, confirming the strong PGE2 binding property of the radiolabeled cyclodextrin probe (Fig. 6. and Table 2). It was also found that the ^{68}Ga-NODAGA-RAMEB accumulation significantly ($p \leq 0.01$) reduced from 30 min to 90 min post injection in most of the investigated thoracic and abdominal organs and BxPC3 tumors (Fig. 6).

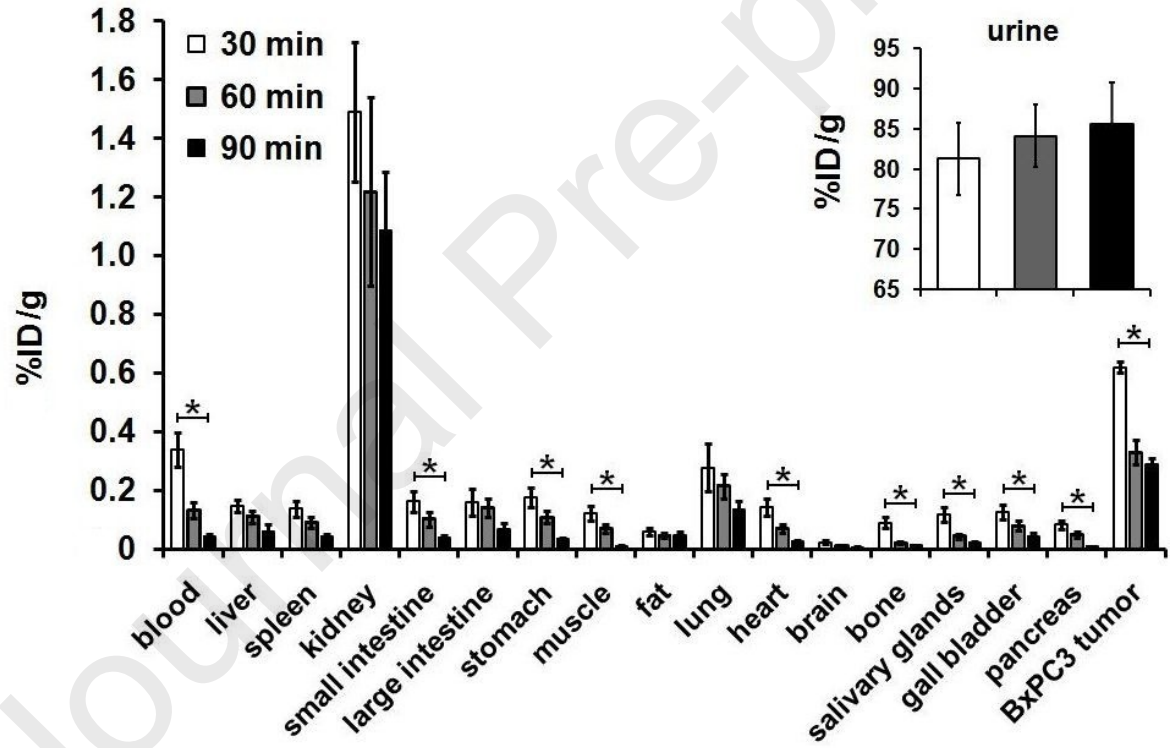

Fig. 6. *Ex vivo* evaluation of ^{68}Ga-NODAGA-RAMEB accumulation in PGE2 positive BxPC3 tumor-bearing CB17 SCID mice (n=15) 30, 60 and 90 min after intravenous injection of the radiotracer and 12±1 days after tumor cell inoculation. Significance level between 30 and 90 min: $p \leq 0.01$ (*). %ID/g values are presented as mean±SD.

Similarly to the *in vivo* PET data, when BxPC3 and PancTu-1 tumors were compared, significantly ($p \leq 0.01$) lower ^{68}Ga-NODAGA-RAMEB accumulation was observed in the PancTu-1 tumors by *ex vivo* measurements 90 min post injection (Table 2). The %ID/g data revealed that approximately 5-fold lower radiotracer uptake was found in PancTu-1 tumors, than that of the accumulation of ^{68}Ga-NODAGA-RAMEB in BxPC3 tumors 90 min post injection. In addition, after the co-injection of ^{68}Ga-NODAGA-RAMEB and PGE2, approximately 20-fold higher tumor uptake (%ID/g) and 6-fold lower T/M ratio were found in BxPC3 tumors at 90 min post injection, than it was observed in the absence of the co-injected PGE2, and this differences were significant ($p \leq 0.01$) (Table 2).

Table 2

Ex vivo assessment of ^{68}Ga-NODAGA-RAMEB uptake (%ID/g) in BxPC3 and PancTu-1 tumors 12±1 days after subcutaneous tumor induction. Significance level between the tumor uptake in the presence and absence of PGE2, and between BxPC3 and PancTu-1 tumors at 90 min: $p \leq 0.01$ (*). 1 mg prostaglandin (PGE2) was co-injected intravenously with ^{68}Ga-NODAGA-RAMEB. T/M: tumor-to-muscle ratio. %ID/g values are presented as mean±SD.

	^{68}Ga-NODAGA-RAMEB		
Tumor	**30min**	**60 min**	**90min**
BxPC3 tumor (n=5)	0.62 ± 0.02	0.33 ± 0.04	0.29 ± 0.02*
BxPC3 with PGE2 (n=5)	-	-	6.71 ± 0.16
BxPC3 T/M	20.03 ± 4.16	15.68 ± 4.04	17.18 ± 3.10*
BxPC3 T/M with PGE2	-	-	2.93 ± 0.46
PancTu-1 tumor (n=5)	-	-	0.06 ± 0.02*
PancTu-1 T/M	-	-	5.40 ± 1.17*

3.8. Immunohistochemistry

After *ex vivo* studies, the presence of prostaglandin E receptor (EP2) was verifiable by immunohistochemistry in the subcutaneously growing BxPC3 and PancTu-1 tumors. Figure 7B shows strong EP2 receptor positivity of the tumor and presents an intensive cytoplasmic/membrane expression throughout the masses of the xenograft pancreas carcinoma cells. In contrast, lower signal intensity was observed during the evaluation of PancTu-1 tumors

(Fig. 7D). These results correlated well with the *ex vivo* and *in vivo* studies, further confirming the strong binding affinity of ^{68}Ga-NODAGA-RAMEB to the PGE2 molecule.

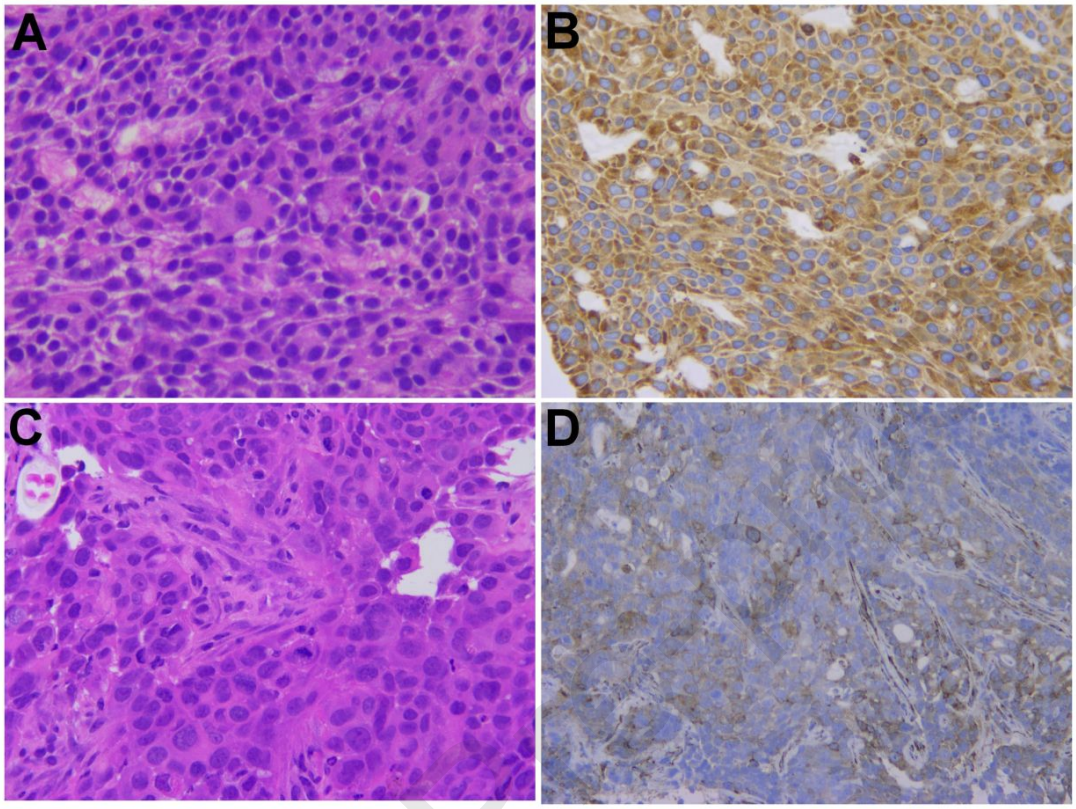

Fig. 7. Histological analysis of subcutaneously growing BxPC3 (A and B panel) and PancTu-1 (C and D panel) tumors 11 days after tumor cell inoculation. A and C: Representative hematoxylin-eosin stained tumor tissue; B and D: Anti-Prostaglandin E Receptor EP2/PTGER2 antibody immunohistochemistry (IHC), visualized with 3,3-diaminobenzidine (DAB) (brown staining). Magnification: 40X.

4. Discussion

In recent years, several studies ascribed a crucial role to Prostaglandin E2 (PGE2) and its G-protein coupled receptors (E series of prostaglandin receptors, EP) in promoting tumor growth, proliferation, migration and development of metastases. Prostaglandin E2 increases tumor proliferation by suppressing the cells of anti-tumor immunity (dendritic cells (DCs), natural killer (NK) and T cells), inhibiting apoptosis and promoting tumor associated neo-angiogenesis (Liu et al., 2015), and all of these effects lead to the survival of tumor cells and the development of distant metastases (Wang and Dubois, 2006). Furthermore, PGE2 may act as a prognostic biomarker of tumors including several cancers (pancreatic cancer, renal, oral and breast cancer (Tong et al., 2018). For these reasons, the *in vivo* detection of PGE2 positive tumors by PET technique with the use of target-specific radiopharmaceuticals may be of great importance.

Sauer and his research group in 2017 found that randomly methylated β-cyclodextrin (RAMEB) had a high affinity to form inclusion complexes with the PGE2 (Sauer et al., 2017). Cyclodextrins are used in several fields of pharmacy and medicine, but they are not used in the field of tumor imaging with positron emission tomography. Our research group previously reported the synthesis a new ^{68}Ga-labeled, and NODAGA chelator modified cyclodextrin derivative (^{68}Ga-NODAGA-HPβCD) and tested the pharmacokinetic properties and *in vivo* distribution of this radiolabeled probe (Hajdu et al., 2019). Based on our previous results, in this present study, NH_2-RAMEB was modified with NODAGA chelating agent and was labeled with Gallium-68 radioisotope to produce a promising radiotracer (^{68}Ga-NODAGA-RAMEB) for *in vivo* PET imaging of PGE2 positive tumors.

For the synthesis of ^{68}Ga-NODAGA-RAMEB molecule, NODAGA chelator was selected, as it is able to form a stable thioureido linkage during the coupling reaction. In this study NODAGA was conjugated to the primary amine of the RAMEB using conventional robust and reproducible coupling protocol (Fig. 1). The radiolabeling procedure was performed similarly to our previous study, and this well-established protocol resulted in a composite material with high radiochemical purity (above 98.0%) and the molar activity of 15.34±1.93 GBq/μmol. Similar results were found when ^{68}Ga-NODAGA-HPβCD was synthesized and characterized by our research group. The radiochemical purity of the ^{68}Ga-NODAGA-HPβCD was also higher than 98%, and the specific activity was approximately 17 GBq/μmol, confirming that our method was optimized for the radiolabeling of cyclodextrin derivatives with ^{68}Ga-NODAGA (Hajdu et al., 2019). The applicability of the radiotracer was evaluated by *in*

vitro and *in vivo* stability studies. The *in vitro* metabolic stability was monitored after 30, 60, 90 and 120 minutes incubation time in order to match the timeframe with the residence of the tracer in the body. The stability test showed that there was no ^{68}Ga loss during the 120 min evaluation period in mouse serum. These results demonstrated that the ^{68}Ga-NODAGA-RAMEB tracer is stable in the presence of serum, which play an important role to consider for intravenous administration. The *in vivo* metabolic stability was determined at 60 min post injection after intravenous administration. The *in vivo* stability results correlated well with the *in vitro* results, as no radio-metabolite was found in the urine. These observations indicate that the newly prepared radiotracer remained stable in the body during the circulation and excretion, and this has been abundantly sufficient for further *in vivo* experiments.

By the determination of partition coefficient, we found that the log*P* value of ^{68}Ga-labeled NODAGA-RAMEB was -3.63±0.04, suggesting that the tracer is highly hydrophilic. The dynamic *in vivo* PET imaging and *ex vivo* biodistribution studies revealed that the ^{68}Ga-NODAGA-RAMEB was mainly excreted by the kidney due to its hydrophilic properties that has been proved by the partition coefficient, in alignment with our other radiolabeled cyclodextrin (^{68}Ga-NODAGA-HPβCD), which was also highly hydrophilic (log*P:*-3.07±0.11) (Hajdu et al., 2019). Figure 3 and Table 1 show, that the accumulation of the tracer in other organs of SCID mice was negligible, and the time-activity curves demonstrated that a fast elimination occured from the body. These results are consistent with those of other researchers, where rapid elimination was also observed through the kidneys by investigations on humans and rats using unlabeled HPβCD and radiolabeled HPβCD (Frijlink et al., 1990; Gould and Scott, 2005; Hajdu et al., 2019). By comparing the *ex vivo* (ID%/g) and *in vivo* (SUVs) biodistribution data of the two ^{68}Ga-labeled cyclodextrin probes, relatively lower ^{68}Ga-NODAGA-RAMEB accumulation was observed in the investigated abdominal and thoracic organs and tissues (Figure 3 and Table 1), than that of the ^{68}Ga-NODAGA-HPβCD (Hajdu et al., 2019). However, the uptake ratio of organs comparing to each other is approximately the same. Furthermore, in case of the ^{68}Ga-NODAGA-RAMEB, relatively high lung accumulation was also observed at each investigated time point by *ex vivo* measurements. The possible reason for this has been already described (Hajdu et al., 2019) for ^{68}Ga-NODAGA-HPβCD, and based on this the highly hydrophilic RAMEB may also accumulate in the water compartments of the lung, and it takes time to return into the circulatory system in mice. However, when biodistribution studies were performed in the presence of PGE2 (^{68}Ga-NODAGA-RAMEB was co-injected intravenously with 1 mg PGE2), we found that the radiotracer was not excreted rapidly from the body, abundance of the radioactivity remained in the body after 90 minutes

post injection (Fig. 4C). One explanation for this observation can be that the ^{68}Ga-NODAGA-RAMEB-PGE2 complex is a moderately enlarged molecule, less hydrophilic (log*P*: approx. -3) and these properties prevent the rapid renal elimination and increases the circulation time in blood vessels. Another reason can be the effect of the interaction of PGE2 with the blood plasma proteins (Raz, 1972), which also can increase the circulation time.

It was published in the literature that prostaglandins tend to form inclusion complex with the beta-CD's (Inoue et al., 2015). We wanted to assess if this complexation takes place also *in vivo* and if this complexation has an influence on the accumulation of the radiolabeled RAMEB in the cancerous tissues, which showed elevated density of PGE receptors. For this reason, we have compared the radiotracer-binging ability of a solid phase resin and a resin conjugated with PGE2. Our measured results support the published hypothesis the PGE2 conjugated resin has bound significantly higher activity than the unmodified resin. This result may prove that PGE2 plays a significant role in the relationship between ^{68}Ga-NODAGA-RAMEB and tumor.

In this present study we have focused on *in vivo* PET imaging to attest the PGE2 selectivity of the ^{68}Ga-labeled NODAGA-RAMEB molecule. For tumor induction in CB17 SCID mice BxPC3 and PancTu-1 cancer cell lines were used. It was earlier reported (Yip-Schneider et al., 2000), that PGE2 production is elevated in BxPC3 human pancreatic adenocarcinoma cell line. Furthermore, it was verified, that the activation of EP1 and EP2 receptors requires significantly higher levels of PGE2 (O'Callaghan and Houston, 2015). Other research group also found strong secretion of PGE2 and high expression of EP2 receptor in BxPC3 cell line, when different human pancreatic cancer cells were characterized by *in vitro* assays (Takahashi et al., 2015). The PGE2 production of PancTu-1 cell line was also investigated. In 2015, Gonnermann's research group verified by flow cytometry and Western Blot analysis, that the COX-2 expression and PGE2 production is very low in PancTu-1 cell line, when different pancreatic ductal adenocarcinoma cells were investigated (Gonnermann et al., 2015). In this study we also found remarkable presence of EP2 receptors in BxPC3 tumors, and lower receptor expression in PancTu-1 tumors, which was verified by immunohistochemistry (Fig. 7), confirming that subcutaneously growing BxPC3 tumors retained this property *in vivo*.

These differences between the BxPC3 and PancTu-1 tumors was clearly visualized by *in vivo* PET imaging (Fig. 5) and *ex vivo* gamma counter measurements (Table 2) after intravenous injection of ^{68}Ga-labeled NODAGA-RAMEB. Since our preliminary experiments with BxPC3 tumors showed that the highest tumor-background ratio (T/M) was observed 80-

90 minutes after the injection of ^{68}Ga-NODAGA-RAMEB (Fig. 4B), PancTu-1 tumors and the effect of the co-injected PGE2 were investigated during this time period in comparative studies. We found, that the accumulation of ^{68}Ga-NODAGA-RAMEB was significantly ($p \leq 0.01$) higher in BxPC3 tumors than in the PancTu-1 tumors characterized by lower EP2 receptor expression and PGE2 production. By analyzing the dynamic PET images, we found, that the highest tumor-background ratio (T/M) was obtained at 80-90 minutes post injection, and this high T/M value greatly influenced the contrast and evaluation of the PET images, and the identification of the tumors. The T/M SUV values of PancTu-1 tumors were approximately 10-fold lower, than those of BxPC3 tumors, confirming the high PGE2 selectivity of the ^{68}Ga-labeled cyclodextrin (Fig. 5B). Moreover, recently a potent and selective prostanoid EP4 receptor antagonist, CJ-042794 was radiolabeled with^{18}F (Zhang et al. 2017). Their result indicated selective tracer accumulation in mice bearing LNCaP prostate cancer xenografts, but the higher uptake remained constant in case of blocking studies also. This outcome can suggest that not the EP4 receptor can play a decisive role in the specific accumulation of the ^{68}Ga-NODAGA-RAMEB in our models.

In our other experiments, after the co-injection of ^{68}Ga-NODAGA-RAMEB and PGE2 different pharmacokinetic properties were observed (Fig. 4). We found that the SUVmean values of BxPC3 tumors were significantly ($p \leq 0.01$) higher (approx. 8-9-fold), than that of the ^{68}Ga-NODAGA-RAMEB accumulation without the co-injected PGE2. In addition, significant radiotracer accumulation was observed in the background tissues. From these data we concluded, that ^{68}Ga-NODAGA-RAMEB-PGE2 complex prevents a rapid renal clearance and increases the circulation time of the radiolabeled RAMEB-PGE2 in blood vessels, resulting a slower, but higher accumulation of ^{68}Ga-NODAGA-RAMEB in BxPC3 tumors.

Overall, our results suggest that there is a strong connection between the PGE2-EP2 and the ^{68}Ga-NODAGA-RAMEB, but the exact targeting mechanism is still not clear. Further investigations are needed to clarify if the radiotracer binds first to PGE2 and then together to the EP2 receptor or ^{68}Ga-NODAGA-RAMEB targets the already EP2 receptor-bound PGE2, or it is also possible that the two processes take place in simultaneously, however, their dynamics are not fully determined. Furthermore, these processes can be greatly influenced by the microenvironment of the tumor, its properties (*e.g.*: prostaglandin production, hypoxia, etc.), and EP2 receptor density. Overall, with the methods used in our study, the following results confirmed the close connection between the PGE2 molecule and ^{68}Ga-NODAGA-RAMEB: 1) the PGE2 conjugated resin bound approx. 20% more ^{68}Ga labeled RAMEB than the unmodified resin; 2) the uptake of ^{68}Ga-NODAGA-RAMEB was significantly higher in

BxPC3 tumors with high EP2 receptor positivity than the PancTu-1 tumors with low expression; 3) the pharmacokinetic properties of ^{68}Ga-NODAGA-RAMEB significantly changed in the presence of the co-injected PGE2 in mice and in BxPC3 tumors.

5. Conclusion

Based on our results, radiolabeled cyclodextrins – as new radiopharmaceuticals – may open a new pathway in the *in vivo* imaging and diagnosis of PGE2 positive tumors, further expanding the applications of cyclodextrins.

Declaration of Competing Interest

The authors declare that they have no known competing financial interests or personal relationships that could have appeared to influence the work reported in this paper.

Acknowledgements

This study was supported by FK_17 (FK124634) research grant of the National Research Development and Innovation Office, Budapest, Hungary and by the János Bolyai Research Scholarship of the Hungarian Academy of Sciences (BO/00365/15 and BO/00290/16). PhD students were supported by the University of Debrecen, Doctoral School of Pharmaceutical Sciences and Doctoral School of Clinical Medicine.

References

Arima, H., Motoyama, K., Higashi, T., 2017. Potential use of cyclodextrins as drug carriers and active pharmaceutical ingredients. Chem. Pharm. Bull. 65(4), 341-348.

Calias, P., 2017. 2-Hydroxypropyl-β-cyclodextrins and the Blood-Brain Barrier: Considerations for Niemann-Pick Disease Type C1. Curr. Pharm. Des. 23, 6231-6238.

Duchene, D., Cavalli, R., Gref, R., 2016. Cyclodextrin-based polymeric nanoparticles as efficient carriers for anticancer drugs. Curr. Pharm. Biotechnol. 17(3), 248-255.

Frijlink, H.W., Visser, J., Hefting, N.R., Oosting, R., Meijer, D.K., Lerk, C.F., 1990. The pharmacokinetics of beta-cyclodextrin and hydroxypropyl-beta-cyclodextrin in the rat. Pharm. Res. 7, 1248-1252.

Frömming, K.H., Szejtli, J., 1994. Cyclodextrins in Pharmacy. Springer

Giovacchini, G., Giovannini, E., Riondato, M., Ciarmiello, A., 2018. PET/CT With 68Ga-PSMA in Prostate Cancer: Radiopharmaceutical Background and Clinical Implications. Curr. Radiopharm. 11, 4-13.

Gonnermann, D., Oberg, H.H., Kellner, C., Peipp, M., Sebens, S., Kabelitz, D., Wesch, D., 2015. Resistance of cyclooxygenase-2 expressing pancreatic ductal adenocarcinoma cells against γδ T cell cytotoxicity. Oncoimmunology. 4, e988460.

Gould, S., Scott, R.C., 2005. 2-Hydroxypropyl-beta-Cyclodextrin (HP-beta-CD): A Toxicology Review. Food Chem. Toxicol. 43, 1451-1459.

Greenhough, A., Smartt, H.J., Moore, A.E., Roberts, H.R., Williams, A.C., Paraskeva, C., Kaidi, A., 2009. The COX-2/PGE2 pathway: key roles in the hallmarks of cancer and adaptation to the tumour microenvironment. Carcinogenesis. 30, 377-386.

Hajdu, I., Angyal, J., Szikra, D., Kertész, I., Malanga, M., Fenyvesi, É, Szente, L, Vecsernyés, M., Bácskay, I., Váradi, J., Fehér, P., Ujhelyi, Z., Vasvári, G., Rusznyák, Á., Trencsényi,

G., Fenyvesi F., 2019. Radiochemical synthesis and preclinical evaluation of 68Ga-labeled NODAGA-hydroxypropyl-beta-cyclodextrin (68Ga-NODAGA-HPBCD). Eur. J. Pharm. Sci. 128, 202-208.

Inoue, Y., Sekiya, N., Yamamoto, M., Iohara, D., Hirayama, F., Uekama, K., 2015. Formation of the Ternary Inclusion Complex of Limaprost with α- and β-Cyclodextrins in Aqueous Solution. Chem. Pharm. Bull. 63, 318-325.

Jiang, J., Qiu, J., Li, Q., Shi, Z., 2017. Prostaglandin E2 Signaling: Alternative Target for Glioblastoma? Trends. Cancer. 3, 75-78.

Koga, H., Sakisaka, S., Ohishi, M., Kawaguchi, T., Taniguchi, E., Sasatomi, K., Harada, M., Kusaba, T., Tanaka, M., Kimura, R., Nakashima, Y., Nakashima O, Kojiro M, Kurohiji, T., Sata, M., 1999. Expression of cyclooxygenase-2 in human hepatocellular carcinoma: relevance to tumor dedifferentiation. Hepatology. 29, 688-696.

Körhegyi, Z., Rózsa, D., Hajdu, I., Bodnár, M., Kertész, I., Kerekes, K., Kun, S., Kollár, J., Varga, J., Garai, I., Trencsényi, G., Borbély, J., 2019. Synthesis of 68Ga-Labeled Biopolymer-based Nanoparticle Imaging Agents for Positron-emission Tomography. Anticancer Res. 39, 2415-2427.

Li, H., Yang, B., Huang, J., Lin, Y., Xiang, T., Wan, J., Li, H., Chouaib, S., Ren, G., 2015. Cyclooxygenase-2 in tumor-associated macrophages promotes breast cancer cell survival by triggering a positive-feedback loop between macrophages and cancer cells. Oncotarget. 6, 29637-29650.

Liu, B., Qu, L., Yan, S., 2015. Cyclooxygenase-2 promotes tumor growth and suppresses tumor immunity. Cancer. Cell. Int. 15, 106.

Loftsson, T., Jarho, P., Másson, M., Järvinen, T., 2005. Cyclodextrins in drug delivery. Expert. Opin. Drug. Deliv. 2, 335-351.

Nagy, G., Dénes, N., Kis, A., Szabó, J.P., Berényi, E., Garai, I., Bai, P., Hajdu, I., Szikra, D., Trencsényi, G., 2017. Preclinical evaluation of melanocortin-1 receptor (MC1-R)

specific 68Ga- and 44Sc-labeled DOTA-NAPamide in melanoma imaging. Eur. J. Pharm. Sci. 106, 336-344.

O'Callaghan, G., Houston, A., 2015. Prostaglandin E2 and the EP receptors in malignancy: possible therapeutic targets? Br. J. Pharmacol. 172, 5239-5250.

Okamatsu, A., Motoyama, K., Onodera, R., Higashi, T., Koshigoe, T., Shimada, Y., Hattori, K., Takeuchi, T., Arima, H., 2013. Folate-appended β-cyclodextrin as a promising tumor targeting carrier for antitumor drugs in vitro and in vivo. Bioconjug. Chem. 24, 724-733.

Ottinger, E.A., Kao, M.L., Carrillo-Carrasco, N., Yanjanin, N., Shankar, R.K., Janssen, M., Brewster, M., Scott, I., Xu, X., Cradock, J., Terse, P., Dehdashti, S.J., Marugan, J., Zheng, W., Portilla, L., Hubbs, A., Pavan, W.J., Heiss, J., Vite, C.H., Walkley, S.U., Ory, D.S., Silber, S.A., Porter, F.D., Austin, C.P., McKew, J.C., 2014. Collaborative development of 2-hydroxypropyl-β-cyclodextrin for the treatment of Niemann-Pick type C1 disease. Curr. Top. Med. Chem. 14, 330-339.

Park, Y.R., Seo, S.Y., Kim, S.L., Zhu, S.M., Chun, S., Oh, J.M., Lee, M.R., Kim, S.H., Kim, I.H., Lee, S.O., Lee, S.T., Kim, S.W., 2018. MiRNA-206 suppresses PGE2-induced colorectal cancer cell proliferation, migration, and invasion by targetting TM4SF1. Biosci. Rep. 38, pii: BSR20180664.

Raz, A., 1972. Interaction of prostaglandins with blood plasma proteins: I. Binding of prostaglandin E2 to human plasma proteins and its effect on the physiological activity of prostaglandin E2 in vitro and in vivo, Biochimica et Biophysica Acta (BBA) - Lipids and Lipid Metabolism. 280, 602-613.

Reader, J., Holt, D., Fulton, A., 2011. Prostaglandin E2 EP receptors as therapeutic targets in breast cancer. Cancer Metastasis Rev. 30, 449-463.

Sauer, R.S., Rittner, H.L., Roewer, N., Sohajda, T., Shityakov, S., Brack, A., Broscheit, J.A., 2017. A Novel Approach for the Control of Inflammatory Pain: Prostaglandin E2 Complexation by Randomly Methylated β-Cyclodextrins. Anesth. Analg. 124, 675-685.

Szejtli, J., 1998. Introduction and general overview of cyclodextrin chemistry. Chem. Rev. 98(5), 1743-1753.

Takahashi, T., Uehara, H., Ogawa, H., Umemoto, H., Bando, Y., Izumi, K., 2015. Inhibition of EP2/EP4 signaling abrogates IGF-1R-mediated cancer cell growth: involvement of protein kinase C-θ activation. Oncotarget. 6, 4829-4844.

Tong, D., Liu, Q., Wang, L.A., Xie, Q., Pang, J., Huang, Y., Wang, L., Liu, G., Zhang, D., Lan, W., Jiang, J., 2018. The roles of the COX2/PGE2/EP axis in therapeutic resistance. Cancer Metastasis Rev. 37, 355-368.

Verratti, V., Brunetti, L., Ferrante, C., Orlando, G., Recinella, L., Chiavaroli, A., Leone, S., Wang, R., Berardinelli, F., 2019. Physiological and pathological levels of prostaglandin E2 in renal parenchyma and neoplastic renal tissue. Prostaglandins Other Lipid Mediat. 141, 11-13.

Wang, D., Dubois, R.N., 2006. Prostaglandins and cancer. Gut. 55, 115-122.

Yip-Schneider, M.T., Barnard, D.S., Billings, S.D., Cheng, L., Heilman, D.K., Lin, A., Marshall, S.J., Crowell, P.L., Marshall, M.S., Sweeney, C.J., 2000. Cyclooxygenase-2 expression in human pancreatic adenocarcinomas. Carcinogenesis. 21, 139-146.

Yokoo, M., Kubota, Y., Motoyama, K., Higashi, T., Taniyoshi, M., Tokumaru, H., ... & Sueoka-Aragane, N. (2015). 2-Hydroxypropyl-β-cyclodextrin acts as a novel anticancer agent. PLoS One, 10, e0141946.

Zhang, Z., Lau. J., Kuo, H.T., Zhang, C., Colpo, N., Bénard, F., Lin, K.S., 2017. Synthesis and evaluation of 18F-labeled CJ-042794 for imaging prostanoid EP4 receptor expression in cancer with positron emission tomography. Bioorg. Med. Chem. Lett. 27, 2094-2098.

Zhou, M., Wang, A., Yin, B., Wu, D., Han, S., Zhang, W., Liu, J., Sun, K., 2019. SND1 promotes the proliferation of osteosarcoma cells by upregulating COX‐2/PGE2 expression via activation of NF‐κB. Oncol. Rep. 41, 579-589.

Zimmer, S., Grebe, A., Bakke, S.S., Bode, N., Halvorsen, B., Ulas, T., Skjelland, M., Nardo, D.D., Labzin, L.I., Kerksiek, A., et al., 2016. Cyclodextrin promotes atherosclerosis regression via macrophage reprogramming. Sci. Transl. Med. 8, 333ra50.

Zmigrodzka, M., Rzepecka, A., Krzyzowska, M., Witkowska-Pilaszewicz, O., Cywinska, A., Winnicka, A., 2018. The cyclooxygenase-2/prostaglandin E2 pathway and its role in the pathogenesis of human and dog hematological malignancies. J. Physiol. Pharmacol. 69, 653-661.

Graphical abstract

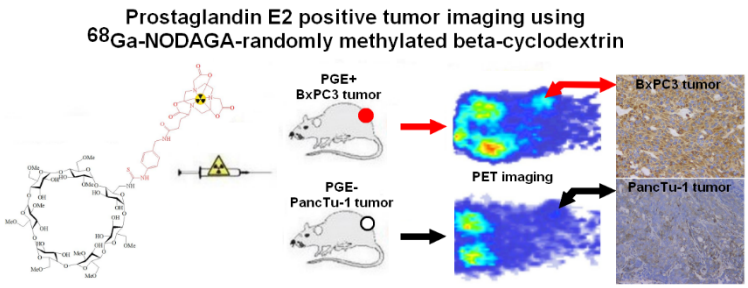

Highlights:

- Prostaglandin E2 (PGE2) specific ^{68}Ga-NODAGA-randomly methylated beta-cyclodextrin (RAMEB) was synthesized
- ^{68}Ga-NODAGA-RAMEB showed high accumulation in BxPC-3 tumors
- The pharmacokinetic properties of ^{68}Ga-NODAGA-RAMEB changed in the presence of PGE2 in BxPC3 tumors
- ^{68}Ga-NODAGA-RAMEB is a promising radiotracer in PET diagnostics of PGE2 positive tumors